Progress In Electromagnetics Research C, Vol. 64, 105–116, 2016

CPW-Fed Phi-Shaped Monopole Antenna for Super-Wideband Applications

Sarthak Singhal* and Amit K. Singh

Abstract—A compact Phi-shaped monopole antenna for super wideband applications is proposed. It consists of a Phi-shaped radiator derived from a conventional elliptical monopole and quarter elliptical CPW ground plane. An impedance bandwidth from 3.5 to 37.2 GHz is achieved with a ratio bandwidth of 10 : 1. It provides an average peak realized gain of 3.5 dB with a group delay of less than 0.5 ns. The proposed antenna structure provides large bandwidth with the advantage of miniaturized dimensions compared to other SWB antenna structures.

1. INTRODUCTION

Recent developments in modern communication systems have excited the need of an antenna which can operate over a bandwidth covering both short- and long-range transmissions for ubiquitous services. These requirements can be fulfilled by a super wideband antenna having a ratio bandwidth of at least 10 : 1 impedance bandwidth at 10-dB return loss. In literature, few super wideband antenna structures [1–10] are available. In most of the structures, super wideband operation is achieved by using fractal concept. Among these SWB structures, planar monopole structures [3–5, 7–10] combine very large bandwidth capabilities with omnidirectional radiation patterns, easy fabrication, and simple integration with the monolithic microwave integrated circuits.

In [1], semielliptical fractal-complementary slots were embedded into the asymmetrical ground plane of a planar microstrip-fed super wideband monopole antenna to achieve a bandwidth of 1.44–18.8 GHz. The dimensions of this antenna were $35 \times 77\,\text{mm}^2$. A probe-fed octagonal fractal microstrip patch antenna covering frequency spectrum from 10 GHz to 50 GHz and having dimensions of $60 \times 60\,\text{mm}^2$ was presented [2]. In [3], a coplanar waveguide-fed monopole antenna composed of a rectangular monopole patch notched at the bottom, a T-shaped CPW ground in the notch, and a tapered CPW ground out of the notch was presented. It had an overall bandwidth of 2.4–24.3 GHz and dimensions of $41 \times 30\,\text{mm}^2$. In a CPW-fed circular monopole antenna, the bandwidth of 0.79–9.16 GHz was achieved by using trapeziform ground planes [4]. In [5], a SWB monopole antenna having bandwidth from 640 MHz to more than 16 GHz and dimensions of $150 \times 150\,\text{mm}^2$ was designed. It comprised a corner rounded partial ground plane and a radiator composed of a semi-elliptical and a semi-circular metallic portions. Circular and elliptical slot antenna structures with both kinds of feeding structures, i.e., microstrip feedline and coplanar waveguide feedline were investigated [6]. All the designed structures covered a bandwidth from approximately 2.65 GHz to more than 20 GHz. In [7], a planar inverted cone antenna (PICA) comprising planar inverted cone radiator and planar inverted cone slot loaded ground plane was proposed. It covered a bandwidth 2.2–25 GHz and had dimensions of $60 \times 60\,\text{mm}^2$. A printed super-wideband (SWB) antenna consisting of an elliptical monopole and a trapezoid ground plane was designed to cover the frequency spectrum from 1.08 GHz to 27.4 GHz [8]. It has dimensions of

Received 24 February 2016, Accepted 27 April 2016, Scheduled 24 May 2016
* Corresponding author: Sarthak Singhal (ssinghal.rs.ece@iitbhu.ac.in).
The authors are with the Department of Electronics Engineering, Indian Institute of Technology (BHU), Varanasi, Uttar Pradesh 221005, India.

$120 \times 124\,\text{mm}^2$. A circular monopole antenna fed by a two stepped microstrip line is designed to cover the frequency spectrum from 3.5 GHz to 31.9 GHz [9]. It had dimensions of $30 \times 35\,\text{mm}^2$. A super wideband (SWB) antenna comprising exponentially tapered feed region and patch printed monopole antenna was designed to cover a bandwidth of 2.5–80 GHz with overall dimensions of $40 \times 30\,\text{mm}^2$ [10]. All these antenna structures had either large dimensions or complex structures or higher frequency limit less or equal to 20 GHz.

In this paper, a Phi-shaped radiator is derived from a conventional elliptical monopole. The area of the proposed antenna structure is $0.2785\lambda \times 0.234\lambda$, where λ is the wavelength at lower cut off frequency of -10 dB return loss bandwidth. The bandwidth of the proposed antenna structure is enhanced by utilizing the techniques of slot loading, addition of tilted metallic strip to the radiator and modified CPW ground plane. It has advantages of large bandwidth with smaller dimensions. This antenna will be suitable for many applications.

2. ANTENNA DESIGN

The configuration of the proposed super wideband antenna structure is depicted in Figure 1. The optimized dimensions of the antenna structure are listed in Table 1. The substrate used for designing the proposed antenna structure is an FR-4 epoxy dielectric material having a dielectric constant of 4.4, loss tangent of 0.02 and thickness of 1.6 mm. From the available literature, it is observed that two kinds of groups work on SWB antenna design. The first group uses an FR-4 substrate due to low fabrication cost and achieving the desirable results [1–10]. On the other hand, the second group has reported the lossy characteristics of an FR-4 substrate at very high frequencies or millimeter wave frequencies [11, 12]. The Phi-shaped radiator is fed by a microstrip line. The initial dimensions of the feedline are calculated by using standard feedline equation [13].

$$50 = \frac{120\pi}{\sqrt{\varepsilon_{reff}}\left[\frac{W_f}{h} + 1.393 + 0.667\ln\left(\frac{W_f}{h} + 1.444\right)\right]} \tag{1}$$

$$\varepsilon_{reff} = \frac{\varepsilon_r + 1}{2} + \frac{\varepsilon_r - 1}{2}\left[1 + 12\frac{h}{W}\right]^{-0.5} \tag{2}$$

Coplanar waveguide ground plane is utilized due to its advantages such as easy fabrication, low loss, convenience for shunt and series connections on the same side of the substrate avoiding via holes, etc.

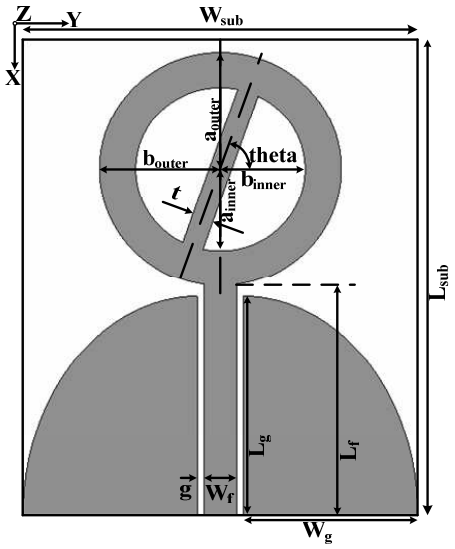

Figure 1. Geometry of the proposed antenna structure.

Table 1. Optimized dimensions of the proposed antenna structure.

Dimension	Value (mm)	Dimension	Value (mm)
L_{sub}	$22(0.2785\lambda)$	W_{sub}	$18.5(0.234\lambda)$
L_f	10.65	W_f	1.5
L_g	10.1	W_g	8.2
a_{outer}	5.4	b_{outer}	$5.67(r_1 \times a_{\text{outer}})$
a_{inner}	$3.78(r_2 \times a_{\text{outer}})$	b_{inner}	$4(r_1 \times a_{\text{inner}})$
r_1	1.05 (unitless)	r_2	0.7 (unitless)
t	1	g	0.3
Theta	70 degree	h	1.6

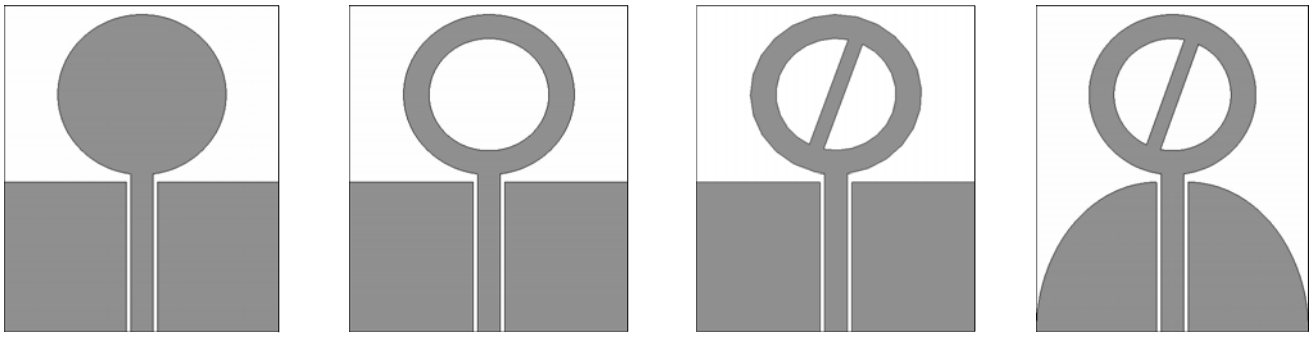

Figure 2. Deriving stages of the Phi-shaped super wideband antenna. (a) Antenna I. (b) Antenna II. (c) Antenna III. (d) Antenna IV.

The structure of the proposed antenna radiator is derived from a conventional elliptical monopole. The deriving stages and structures of the proposed antenna are demonstrated in Figure 2. Initially an elliptical monopole antenna with rectangular CPW ground plane, shown in Figure 2(a), is designed and investigated. Since the current density at the central part of ellipse is zero or negligible, an elliptical slot is etched to produce an annular ring radiator, demonstrated in Figure 2(b). After this slot loading, a tilted rectangular strip is added to the annular radiator resulting into Phi-shaped radiator, shown in Figure 2(c). Thereafter, the conventional rectangular CPW ground plane is replaced by quarter elliptical CPW ground planes, shown in Figure 2(d). All the simulations are carried out by using FEM-based Ansoft's HFSS simulation software [14].

3. RESULTS AND DISCUSSION

The comparison among the reflection coefficients of antenna structures designed at various derivation stages of the proposed antenna versus frequency is shown in Figure 3 and listed in Table 2. From Figure 3 and Table 2, it is observed that antenna I has four operating bands, i.e., 4.47–5.56 GHz, 7–11.82 GHz, 12.9–20.9 GHz and 22.33–40 GHz. It has eight resonances at the frequencies of 5, 8.34, 9.84, 14.24, 17.9, 23.52, 29.31 and 34.85 GHz. After the loading of elliptical radiator with elliptical slot resulting in antenna II, the number of resonances gets increased from eight (5, 8.34, 9.84, 14.24, 17.9, 23.52, 29.31 and 34.85 GHz) to nine (5, 7.37, 10.16, 14.24, 17.78, 23.47, 29.6, 31.63 and 34.47 GHz), and the lower cutoff frequency of the first operating band is decreased from 4.47 GHz to 4.27 GHz. In this case, the number of operating bands is also unchanged, i.e., four. The bandwidth of the first operating band is enhanced from 1.09 GHz to 4.08 GHz whereas the bandwidth of the second operating band is decreased

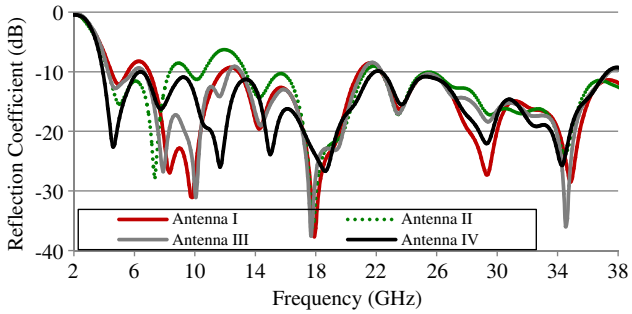

Figure 3. Variation of reflection coefficient with frequency for deriving stages of the proposed antenna structure.

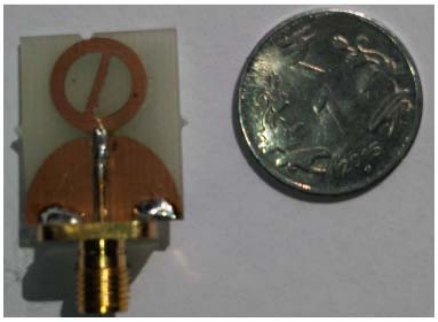

Figure 4. Prototype of the designed antenna.

Table 2. Tabulated comparison of bandwidth of deriving stages of the proposed antenna structure.

Antenna	I	II	III	IV
f_{L1} (GHz)	4.47	4.27	4.27	3.8
f_{H1} (GHz)	5.56	8.35	5.93	38
Bandwidth (BW1) (GHz)	1.09	4.08	1.66	34.2
f_{L2} (GHz)	7	9.59	6.62	-
f_{H2} (GHz)	11.82	10.59	12.28	-
Bandwidth (BW2) (GHz)	4.82	1	5.66	-
f_{L3} (GHz)	12.9	13.35	13	-
f_{H3} (GHz)	20.9	21.3	21.07	-
Bandwidth (BW3) (GHz)	8	7.95	8.07	-
f_{L4} (GHz)	22.33	22.32	22.37	-
f_{H4} (GHz)	40	40	40	-
Bandwidth (BW4) (GHz)	17.67	17.68	17.63	-

from 4.84 GHz to 1 GHz. The lower and higher edge frequencies of the third operating band are shifted from 12.9 GHz to 13.35 GHz and 20.9 GHz to 21.3 GHz with no significant effect on the bandwidth. The fourth operating band is unaffected by this slot loading. For antenna III, i.e., after the addition of tilted rectangular strip to the radiator of antenna II, the first operating band again gets reduced from 4.08 GHz to 1.66 GHz whereas the second operating band is widened from 1 GHz to 5.66 GHz, and the last two operating bands are observed to be unaffected. Three additional resonances at the frequencies of 11.66, 19.28 and 27.334 GHz are achieved along with the shifting of previously obtained resonances. After this, by replacing the conventional CPW rectangular ground plane with quarter elliptical ground plane, all the previously defined four operating bands are merged resulting into a single operating band ranging from 3.8 to 38 GHz.

The proposed SWB antenna structure is fabricated using T-Tech QC-5000 micro-milling machine after the verification of the results obtained from FEM based HFSS software, by using the CST MWS software [15]. The final prototype is shown in Figure 4. The experimental measurement of the reflection coefficient and VSWR characteristics is carried out by using Agilent E8364B PNA. The comparison between the experimental and simulated reflection coefficients versus frequency is depicted in Figure 5. The tabular comparison of experimental and simulation results is listed in Table 4. A good agreement is observed between the experimental and simulation results. Similar observations are made from the comparison of measured and simulated VSWR results, demonstrated in Figure 6. The discrepancies between the HFSS and CST results are due to the different mesh sizes of two simulators suitable for

Table 3. Tabulated comparison of resonances of deriving stages of the proposed antenna structure.

Antenna	I	II	III	IV
f_1 (GHz)	5	5	4.69	4.58
f_2 (GHz)	8.34	7.37	7.91	7.8
f_3 (GHz)	9.84	10.16	10.05	11.67
f_4 (GHz)	14.24	14.24	11.66	15
f_5 (GHz)	17.9	17.78	14.35	18.64
f_6 (GHz)	23.52	23.47	17.67	23.69
f_7 (GHz)	29.31	29.6	19.28	29.27
f_8 (GHz)	34.85	31.63	23.47	32.59
f_9 (GHz)	-	34.47	27.334	34.31
f_{10} (GHz)	-	-	29.37	-
f_{11} (GHz)	-	-	32.486	-
f_{12} (GHz)	-	-	34.53	-

Table 4. Tabulated comparison between the measured and simulated results of the proposed antenna structure.

Software	f_L (GHz)	f_H (GHz)	BW (GHz)
CST MWS	3.8	38	34.2
HFSS	3.8	37	33.2
Measured	3.5	37.2	33.7

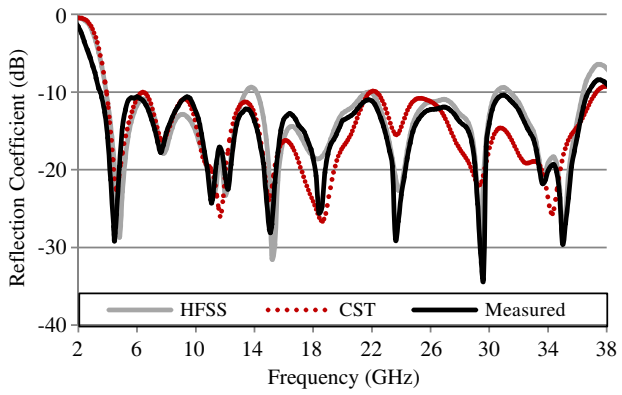

Figure 5. Comparison between the measured and simulated reflection coefficient versus frequency plots of the proposed antenna structure.

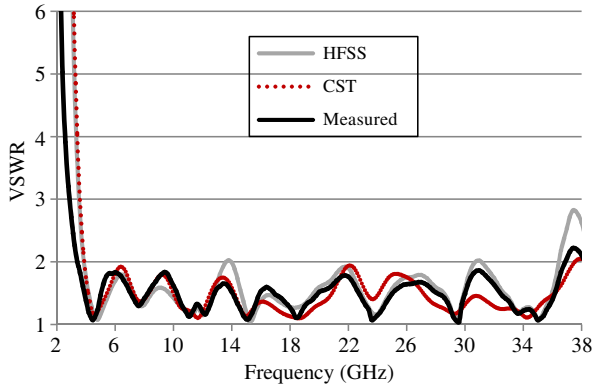

Figure 6. Comparison between the measured and simulated VSWR versus frequency plots of the proposed antenna structure.

their different analytical techniques. In CST MWS, the antenna response for the whole frequency range is achieved in a single pass, whereas in HFSS, the antenna response is achieved by dividing the operating range into multiple parts. The disparity between the experimental and simulated results can be attributed to the fabrication tolerances and imperfect soldering effects of SMA.

A comparison between two wideband antennas is done in terms of ratio bandwidth, 10-dB bandwidth, electrical dimension, and Bandwidth Dimension Ratio (BDR). The index term BDR allows antenna engineers to identify the compactness and wider bandwidth characteristics of their

Table 5. Comparison of designed antenna with other super wideband antenna structures.

S. No.	Antenna Type	Ratio BW	10-dB BW(%)	Electrical Dimension	BDR	f_{low} (GHz)
1.	[1]	13.06 : 1	172	$0.17\lambda \times 0.37\lambda$	2735	1.44
2.	[2]	5 : 1	133	$2\lambda \times 2\lambda$	33.33	10
3.	[3]	10.31 : 1	165	$0.23\lambda \times 0.32\lambda$	2230	2.20
4.	[4]	21.25 : 1	167	$0.37\lambda \times 0.24\lambda$	1876	0.79
5.	[5]	25 : 1	185	$0.32\lambda \times 0.34\lambda$	1682	0.64
6.	[6]	15.38 : 1	175	$0.38\lambda \times 0.38\lambda$	1250	1.30
7.	[7]	13.63 : 1	172	$0.44\lambda \times 0.44\lambda$	905	2.20
8.	[8]	25 : 1	184.83	$0.432\lambda \times 0.45\lambda$	950.77	1.08
9.	[9]	9.11 : 1	160.45	$0.41\lambda \times 0.29\lambda$	1347.24	3.5
10.	**Proposed Antenna**	**10:1**	**164**	$\mathbf{0.2785\lambda \times 0.234\lambda}$	**2541.12**	**3.8**

designed antenna in comparison to other structures. BDR indicates how much operating bandwidth (in percentage) can be provided per electrical area unit (unit: $\%/\lambda^2$) [1]. It is defined as follows:

$$\text{BDR} = \frac{\text{Bandwidth}\%}{\lambda_{\text{length}} \times \lambda_{\text{width}}} \tag{3}$$

where, λ is the wavelength at the lower cut off frequency of the operating bandwidth. A large value of BDR is desirable to verify the advantages of the proposed antenna structure over already available structures in terms of size and bandwidth. The results of the comparison between the proposed antenna structure and other antenna structures [1–9] are presented in Table 5. From Table 5, it is observed that the proposed antenna structure has lower ratio bandwidth than other structures. It is also observed that a BDR of 2541 is exhibited by the designed antenna. Therefore, it can be concluded that good bandwidth characteristics with much smaller dimensions are offered by this antenna in comparison to other antennas [1–9].

Figure 7 demonstrates the variation of real and imaginary parts of simulated input impedance of the proposed antenna structure with frequency. From Figure 7, it is observed that the real part oscillates around $50\,\Omega$ whereas the imaginary part oscillates around $0\,\Omega$ in the operating bandwidth. These oscillations provide an observation that the overall input impedance of this antenna structure is approximately $50\,\Omega$, i.e., the characteristic impedance of the coaxial probe. This equivalence in impedance values will result in better transfer of power from the coaxial probe to the feedline.

The measurement setup for the radiation pattern of designed antenna structure is shown in Figure 8. The antenna structure points in $\Phi = 0^\circ$ direction while lying along X-axis in X-Y plane. θ is varied from 0° to 360° to measure E-plane and H-plane patterns in X-Z plane and Y-Z plane, respectively.

The radiation patterns of the proposed antenna in both E-plane ($\Phi = 0^\circ$) and H-plane ($\Phi = 90^\circ$) are measured in an anechoic chamber. During the measurement, pyramidal horns are used as transmitting antennas. The transmitting antennas are connected to Microwave Analog Signal Generator through an isolator and waveguide to coaxial transitions for corresponding frequency bands. The proposed antenna, to be used as receiving antenna, is connected to coaxial detector and placed in far-field region.

The simulated and measured radiation patterns of the proposed antenna structure at three frequencies in two planes, i.e., E-plane ($\Phi = 0^\circ$) and H-plane ($\Phi = 90^\circ$), are demonstrated in Figure 9. For the first frequency at 4.6 GHz, shown in Figure 9(a), it is observed that the H-plane pattern is omnidirectional whereas the E-plane pattern is bidirectional. For the remaining frequencies greater than 10 GHz, distorted omnidirectional patterns are observed in both planes. The distortion of patterns at higher frequencies can be attributed to the higher modes occurring at corresponding frequencies. In these radiation patterns, normalized gain is plotted.

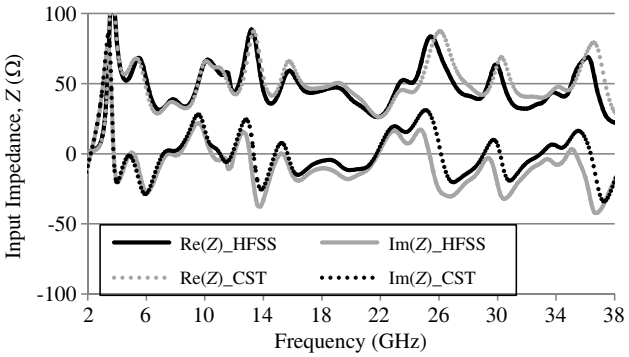

Figure 7. Variations of real and imaginary parts of simulated input impedance of proposed antenna structure.

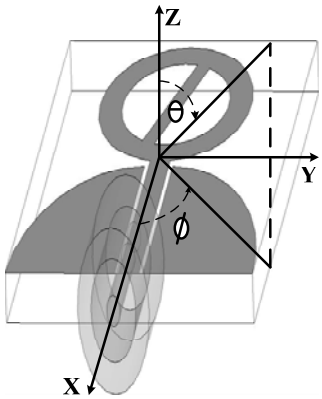

Figure 8. Radiation pattern measurement setup for Phi shaped monopole antenna.

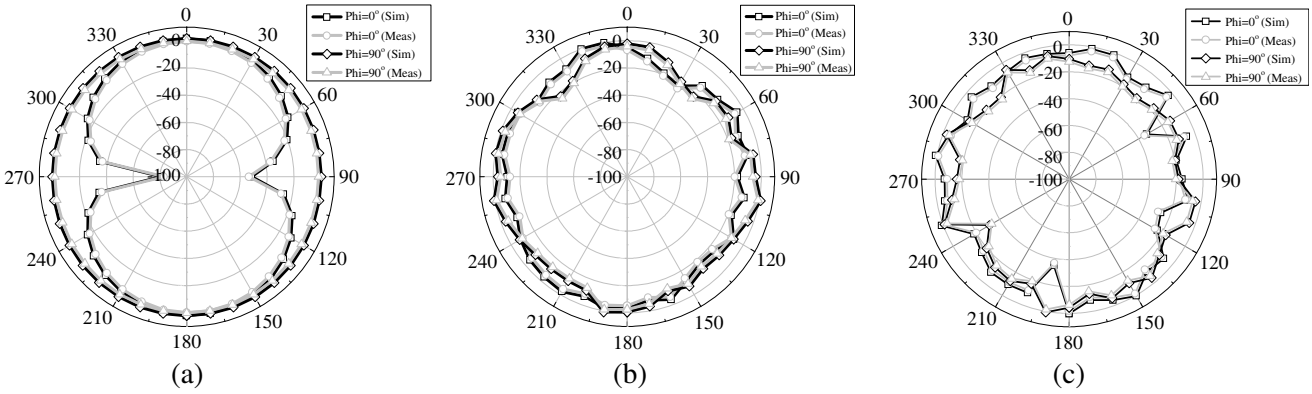

Figure 9. Simulated and measured radiation patterns of the designed antenna structure at some frequencies in both planes. (a) 4.6 GHz. (b) 18.6 GHz. (c) 34.3 GHz.

The variation of experimental peak realized gain of the designed antenna structure is given in Figure 10. From Figure 10, it is observed that the peak realized gain increases with frequency. This phenomenon takes place because at higher frequencies the dimensions of radiating patch are larger than the wavelength corresponding to that higher frequency. The measured peak gain has a minimum of 1.89 dB at 3.8 GHz and 13.7 dB at 33 GHz. These values of peak gain are in accordance with the peak gain reported in previous SWB structures [2, 10, 16].

The plots of total and radiation efficiencies of the proposed antenna structure versus frequency are depicted in Figure 11. It leads to an observation that this antenna structure has a radiation efficiency varying between 0.55 and 0.99. The total efficiency has a variation from 0.50 to 0.94. Both efficiencies are observed to decrease with increase in frequency. It is because at various frequencies there are varying performances of the radiating structure, substrate and SMA connector.

The distribution of current density along the surface of the proposed antenna structure is studied by simulating it. It is observed that for the first resonance of 4.6 GHz, shown in Figure 12(a), the current density is high at the transition from the feedline to the radiator and at the lower portion of ground plane around the feedline. In the remaining portion of the structure, the surface current is uniformly distributed. At the second resonance, depicted in Figure 12(b), current is observed to be highly concentrated around the upper section of feedline, at the transition between the feedline and radiator. Low current density is observed at some sections in radiator, titled strip and ground plane. In the case of third resonance, demonstrated in Figure 12(c), the current density is high around the

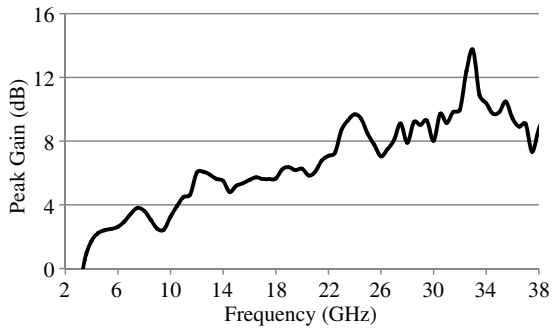

Figure 10. Measured peak realized gain versus frequency characteristics of the designed antenna structure.

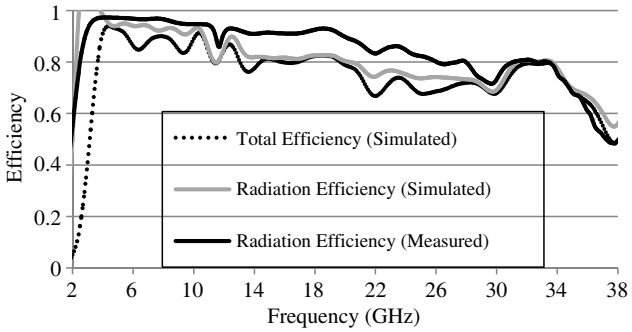

Figure 11. Total and radiation efficiencies versus frequency characteristics of the designed antenna structure.

Table 6. Fidelity factor of the designed antenna in two configurations of time domain analysis.

Configuration	Face to Face	Side by Side
Fidelity Factor (%)	75	80

whole length of feedline, in the left half section of annular ring and inside the tilted strip. Zero surface current density is observed in the middle portion of ground plane. For the fourth resonance, shown in Figure 12(d), high current density is observed in and around the feedline. Uniform current density distribution is found along the whole antenna structure. The area of zero current density surface in the ground plane is much less than that in the case of the third resonance. At the fifth resonance of 18.6 GHz, presented in Figure 12(e), the surface current density distribution is similar to that of the fourth resonance except the zero density at the upper portion of radiator. In the case of the sixth resonance, depicted in Figure 12(f), the surface current density distribution is almost unaffected except the increase in the area of zero current density surface inside the ground plane. For the seventh resonance, shown in Figure 12(g), the current density inside the radiator is increased, and the area of zero current density surfaces in the ground plane is also increased. At the eighth resonance, demonstrated in Figure 12(h), the zero current surfaces are observed to be shifted from the ground plane to the tilted strip of radiator. In the case of last resonance, depicted in Figure 12(i), almost no small zero current density surfaces are observed inside the ground plane.

During the time domain analysis of the proposed structure, a distance of 15 cm is kept between two similar antenna structures in two configurations, i.e., face to face and side by side. The two configurations are illustrated in Figure 13. Each antenna structure is excited by a Gaussian pulse, having centre frequency of 20.25 GHz and bandwidth of 0.5–40 GHz, to act as a transmitter, and the transmitted impulse is received at the second antenna structure. The normalized amplitudes of transmitted and received pulses in both configurations are shown in Figure 14. By using these normalized amplitudes of both configurations, a well-defined term Fidelity Factor (FF) is calculated by using the following equation [17]:

$$\mathrm{FF} = \max\left[\frac{\int_{-\infty}^{\infty} s_t(t)s_r(t+\tau)d\tau}{\int_{-\infty}^{\infty}|s_t(t)|^2\,dt\int_{-\infty}^{\infty}|s_r(t)|^2\,dt}\right] \tag{4}$$

where, $s_t(t)$ and $s_r(t)$ are the transmitted and received pulses, and τ is the group delay. This fidelity factor defines the amount of correlation between the transmitted and received pulses. The calculated values of the fidelity factor in both configurations are listed in Table 6. From Table 6, it can be concluded that in side by side configuration the correlation is more than that in face to face configuration. This observation implies that the antenna transmits the exciting pulse with less distortion in side by side configuration and with more distortion in another configuration.

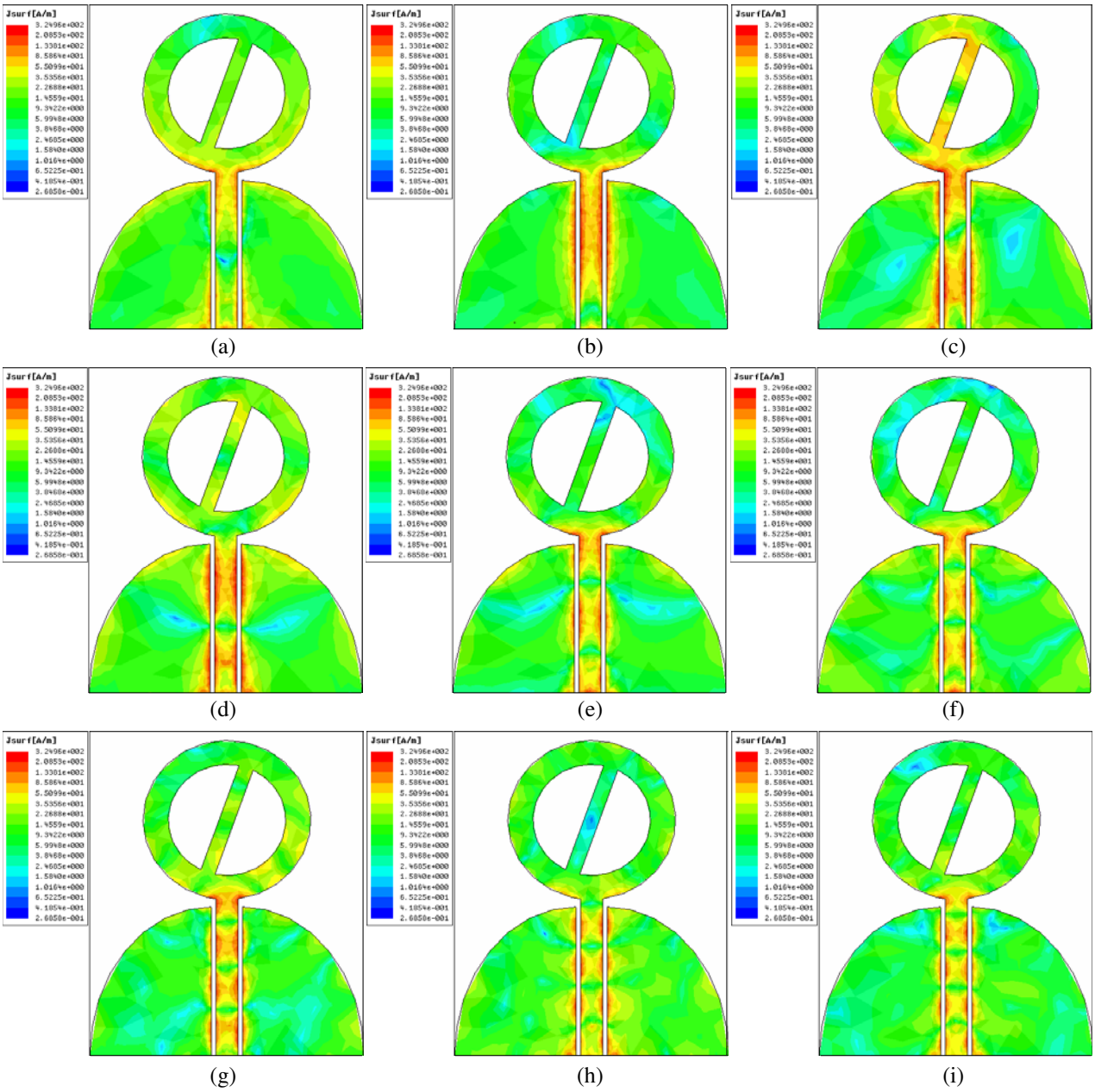

Figure 12. Simulated surface current density plots of the designed antenna structure at its resonance frequencies. (a) 4.6 GHz. (b) 7.8 GHz. (c) 11.7 GHz. (d) 15 GHz. (e) 18.6 GHz. (f) 23.7 GHz. (g) 29.3 GHz. (h) 32.6 GHz. (i) 34.3 GHz.

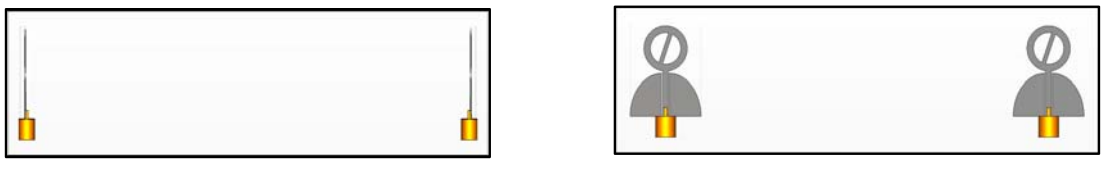

Figure 13. Time domain analysis configurations of the Phi shaped monopole antenna. (a) Face to Face. (b) Side by Side.

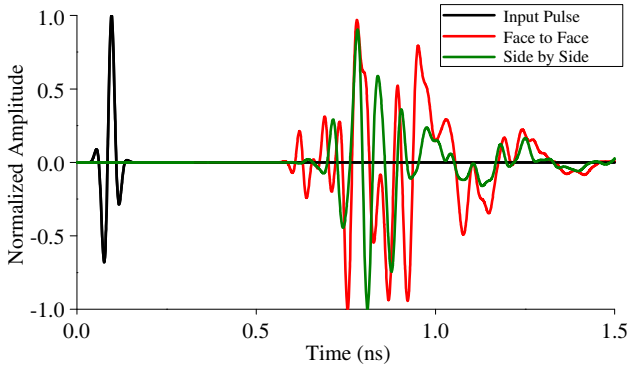

Figure 14. Simulated normalized magnitude of transmitted and received pulses versus time characteristics of the designed antenna structure in two configurations.

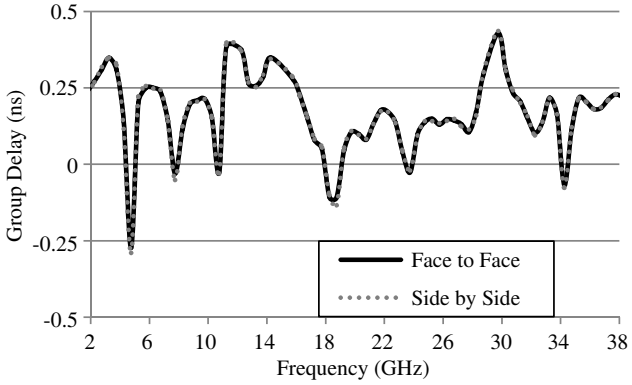

Figure 15. Simulated group delay versus frequency characteristic of the designed antenna structure.

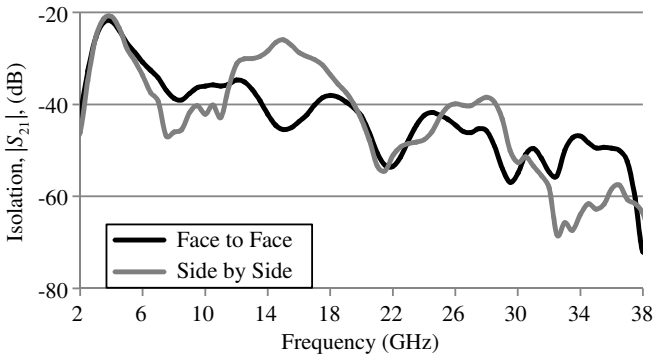

Figure 16. Simulated magnitude of isolation, S_{21}, versus frequency characteristics of the designed antenna structure.

Group delay is defined as the negative rate of change of transfer function phase with respect to frequency and is mathematically calculated by using the following equation [18]. It is a measure of signal transition time through a device.

$$\tau_g(\omega) = -\frac{d\phi(\omega)}{d\omega} = -\frac{d\phi(\omega)}{2\pi df} \tag{5}$$

where, Φ is the phase response of the radiated signal and ω the frequency in radians per second. The phase response and group delay are related to the antenna gain response. The simulated group delay in both configurations is shown in Figure 15. Figure 15 leads to an observation that the group delay varies between -0.3 ns and 0.4 ns. These limits of group delay are in a acceptable range for wideband applications.

The antenna transfer function is expressed as

$$H(\omega) = \sqrt{\frac{2\pi RcS_{21}(\omega)e^{j\omega R/c}}{j\omega}} \tag{6}$$

where, c is the free space velocity and R the distance between the two antennas [19]. The variation of the amplitude of simulated isolation, S_{21}, with frequency in both configurations is shown in Figure 16. From Figure 16, it is observed that the isolation amplitude varies from -20 to -70 dB for both configurations. The phase of the isolation, S_{21}, shown in Figure 17, for both configurations also varies linearly with frequency, leading to the observation that there will be no phase shift in the transmitted pulse.

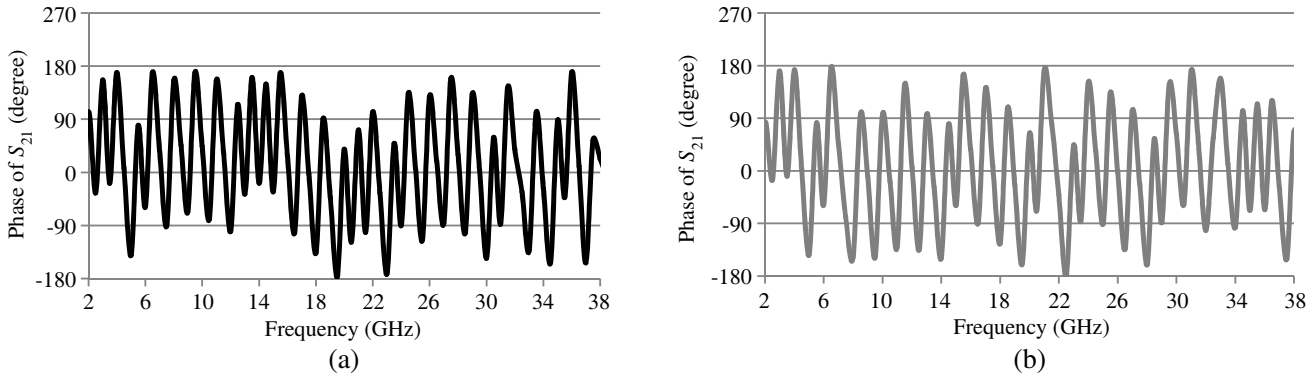

Figure 17. Simulated phase of S_{21} versus frequency characteristics of the designed antenna structure. (a) Face to Face. (b) Side by Side.

4. CONCLUSION

A Phi-shaped monopole antenna for super-wideband applications is designed and analyzed. The designed antenna structure is derived from a conventional CPW-fed elliptical monopole antenna. The validation of simulated results by the experimental results justifies the suitability of this antenna structure for SWB applications. The comparison of the designed antenna structure with other antenna structures available in the literature is done in terms of a well-defined term, BDR. The comparison in terms of BDR verifies the advantages of miniaturized size and wide bandwidth provided by this antenna structure over other antenna structures. Due to those advantages, this antenna structure will be useful for UWB applications, mobile applications, WAS/RLANS (17.1–17.3 GHz), satellite applications, defence systems, BBDR (4.94–4.99 GHz), radio determination applications (4.5–7 GHz, 13.4–14 GHz), Doppler Navigation aids, radio astronomy (22.5 GHz, 24.05–27 GHz, 36.43–36.50 GHz), SRR (21.4–27 GHz), ISM (24.25 GHz), Wideband High Definition Television, Aeronautical Radio Navigation, VSAT/SNG etc. [20].

ACKNOWLEDGMENT

Sarthak Singhal is very thankful to the Ministry of Human Resource & Development, Government of India, for providing the financial support in the form of Teaching Assistantship.

REFERENCES

1. Chen, K. R., C. Y. D. Sim, and J. S. Row, "A compact monopole antenna for super wideband applications," *IEEE Antennas and Wireless Propagation Letters*, Vol. 10, 488–491, 2011.
2. Azari, A., "A new super wideband fractal microstrip antenna," *IEEE Transactions on Antennas and Propagation*, Vol. 59, No. 5, 1724–1727, May 2011.
3. Deng, C., Y. J. Xie, and P. Li, "CPW-fed planar printed monopole antenna with impedance bandwidth enhanced," *IEEE Antennas and Wireless Propagation Letters*, Vol. 8, 1394–1397, 2009.
4. Liang, X. L., S. S. Zhong, and W. Wang, "UWB printed circular monopole antenna," *Microwave and Optical Technology Letters*, Vol. 51, No. 4, 1532–1534, Aug. 2006.
5. Dong, Y., W. Hong, L. Liu, Y. Zhang, and Z. Kuai, "Performance analysis of a printed super-wideband antenna," *Microwave and Optical Technology Letters*, Vol. 51, No. 4, 949–956, Apr. 2009.
6. Angelopoulos, E. S., A. Z. Anastopoulos, D. I. Kaklamani, A. A. Alexandridis, F. Lazarakis, and K. Dang, "Circular and elliptical CPW-fed slot and microstrip-fed antennas for ultrawideband applications," *IEEE Antennas and Wireless Propagation Letters*, Vol. 5, 294–297, 2006.

7. Cheng, S., P. Hallbjörner, and A. Rydberg, "Printed slot planar inverted cone antenna for ultrawideband applications," *IEEE Antennas and Wireless Propagation Letters*, Vol. 7, 18–21, 2008.
8. Liu, J., K. P. Esselle, S. G. Hay, and S. Zhong, "Achieving ratio bandwidth of 25 : 1 from a printed antenna using a tapered semi-ring feed," *IEEE Antennas and Wireless Propagation Letters*, Vol. 10, 1333–1336, 2011.
9. Srifi, M. N., S. K. Podilchak, M. Essaaidi, and Y. M. M. Antar, "Compact disc monopole antennas for current and future ultrawideband (UWB) applications," *IEEE Transactions on Antennas and Propagation*, Vol. 59, No. 12, 4470–4480, Dec. 2011.
10. Manohar, M., R. S. Kshetrimayum, and A. K. Gogoi, "Printed monopole antenna with tapered feed line, feed region and patch for super wideband applications," *IET Microwaves, Antennas & Propagation*, Vol. 8, No. 1, 39–45, 2014.
11. Manohar, M., R. S. Kshetrimayum, and A. K. Gogoi, "Super wideband antenna with single band suppression," *International Journal of Microwave and Wireless Technologies*, Cambridge University Press and the European Microwave Association, 1–8, 2015, doi:10.1017/S1759078715000963.
12. Huang, Y. and K. Boyle, *Antennas from Theory to Practice*, 64, John Wiley & Sons, West Sussex, UK, 2008.
13. Balanis, C. A., *Antenna Theory: Analysis and Design*, 3rd Edition, Wiley India Edition, 2012.
14. HFSS, "High frequency structure simulator ver. 11, finite element package," Ansoft Corporation, available: http://www.ansoft.com, 2009.
15. CST Microwave Studio Suite 2011, CST Inc., 2007.
16. Shahu, B. L., S. Pal, and N. Chattoraj, "Design of super wideband hexagonal-shaped fractal antenna with triangular slot," *Microwave and Optical Technology Letters*, Vol. 57, No. 7, 1659–1662, Jul. 2015.
17. Quintero, G., J. F. Zurcher, and A. K. Skrivervik, "System fidelity factor: A new method for comparing UWB antennas," *IEEE Transactions on Antennas and Propagation*, Vol. 59, No. 7, 2502–2512, 2011.
18. Weisbeck, W., G. Adamiuk, and C. Sturm, "Basic properties and design principles of UWB antennas," *Proceedings of the IEEE*, Vol. 97, No. 2, 372–385, Feb. 2009.
19. Sorgel, W. and W. Weisbeck, "Influence of the antennas on the ultrawideband transmission," *EURASIP Journal of Applied Signal Processing*, Vol. 3, 296–305, 2005.
20. "The European table of frequency allocations and applications," ERC Report 25, approved in May 2014.